Retrieval of cirrus properties by Sun photometry: A new perspective on an old issue

Michal Segal-Rosenheimer,[1] Philip B. Russell,[1] John M. Livingston,[2] S. Ramachandran,[3] Jens Redemann,[1] and Bryan A. Baum[4]

Received 20 September 2012; revised 8 January 2013; accepted 11 January 2013; published 20 May 2013.

[1] Cirrus clouds are important modulators of the Earth radiation budget and continue to be one of the most uncertain components in weather and climate modeling. Sun photometers are widely accepted as one of the most accurate platforms for measuring clear sky aerosol optical depth (AOD). However, interpretation of their measurements is ambiguous in the presence of cirrus. Derivation of a valid AOD under cirrus conditions was focused previously on correction factors, rather than on derivation of cirrus cloud optical thickness (COT). In the present work, we propose a new approach that uses the total measured irradiance to derive cirrus COT and ice particle effective diameter (D_{eff}). For this approach, we generate lookup tables (LUTs) of total transmittance for the Sun photometer field of view (FOV) due to the direct and scattered irradiance over the spectral range of 400–2200 nm, for a range of cirrus COT (0–4), and a range of ice cloud effective diameters (10–120 μm) by using explicit cirrus optical property models for (a) cirrus only and (b) a two-component model including cirrus and aerosols. The new approach is tested on two cases (airborne and ground-based) using measured transmittances from the 14-channel NASA Ames Airborne Tracking Sun photometer. We find that relative uncertainties in COT are much smaller than those for D_{eff}. This study shows that for optically thin cirrus cases (COT < 1.0), the aerosol layer between the instrument and the cloud plays an important role, especially in derivation of D_{eff}. Additionally, the choice of the cirrus model may introduce large differences in derived D_{eff}.

Citation: Segal-Rosenheimer, M., P. B. Russell, J. M. Livingston, S. Ramachandran, J. Redemann, and B. A. Baum (2013), Retrieval of cirrus properties by Sun photometry: A new perspective on an old issue, *J. Geophys. Res. Atmos.*, *118*, 4503–4520, doi:10.1002/jgrd.50185.

1. Introduction

[2] Quantification of cirrus microphysical and optical properties, either by in situ measurements or remote-sensing platforms, is an ongoing effort that continues to gain much attention. Ice clouds (e.g., cirrus), which cover more than 30% of the globe at any time [e.g., *Liou*, 1986; *Wylie and Menzel*, 1999], are important modulators of the Earth climate and radiation budget and are still one of the most uncertain components in weather and climate studies and in the quantification of warming or cooling effects [*DeMott et al.*, 2010; *Nazaryan et al.*, 2008]. Although immense progress has been made toward better and more accurate retrievals of cirrus properties (e.g., optical thickness, cloud effective particle size), large uncertainties still remain. A recent comparison study [*Comstock et al.*, 2007] examined various ground-based instruments and retrieval algorithms of cloud optical thickness (COT) and showed differences in derived optical thickness of up to one order of magnitude for optically thin cirrus (COT < 0.3) and large differences even for relatively optically thicker cirrus (0.3 < COT < 5).

[3] Although several satellite instruments provide cirrus optical thickness (e.g., CALIPSO, MODIS) and effective ice crystal diameter (e.g., MODIS) operationally, airborne and ground-based platforms can expand this capability by providing retrievals at a higher spatial and temporal resolution, respectively. The Sunphotometer is a good example of a versatile instrument that is relatively simple to operate and calibrate and is available both on airborne (e.g., AATS-14—14-channel Ames Airborne Tracking Sun photometer [*Russell et al.*, 2005]) and ground-based platforms (e.g., AERONET [*Holben et al.*, 2001]). Because of their ease of use and their implementation in many countries, both as airborne and ground-based instruments, Sun photometers have the potential to contribute significantly to quantifying some of the most important cirrus properties such as COT and ice crystal effective diameter.

[4] Under thin cirrus, the direct incoming solar radiation can reach the Sun photometer detector, but this feature was never exploited as a means for cirrus COT retrievals. In fact, such measurements are usually excluded from the final aerosol

[1]NASA Ames Research Center, Moffett Field, California, USA.
[2]SRI International, Menlo Park, California, USA.
[3]Physical Research Laboratory, Ahmedabad, India.
[4]Space Science and Engineering Center, University of Wisconsin-Madison, Madison, Wisconsin, USA.

Corresponding author: M. Segal-Rosenheimer, NASA Ames Research Center, Moffett Field, CA, USA. (michal.segalrozenhaimer@nasa.gov)

2169-897X/13/10.1002/jgrd.50185

optical depth (AOD) product derived from these instruments. The reason is that the Sun photometer's field of view (FOV), although generally relatively narrow, will always exceed the Sun's subtended angular half-width (which is 0.25°) and potentially result in decreased tracking performance under cloudy conditions (here we are excluding instruments that view only a portion of the solar disk, like the spaceborne limb-viewing SAGE instruments). Under cloudy conditions in general, and under cirrus in particular, such instruments admit light from at least a part of the strong forward scattering peak of the cloud particles, thus increasing the incoming radiation that is measured in the detector beyond the direct solar transmittance [*Kinne et al*., 1997]. This higher transmittance leads to an underestimation of the derived total column optical depth (aerosol plus cloud) and to an overestimation of AOD if the cloud contribution is not taken into account. Several investigations [*Shiobara and Asano*, 1994; *Kinne et al*., 1997] have attempted to account for this increased radiation amount and to derive a correction factor for the retrieved AOD. Even the AERONET Fine Mode Fraction (FMF) retrieved value [*O'Neill et al*., 2003], which represents the optical depth ratio of fine mode to the total optical depth, is based on the total uncorrected optical depth when cirrus is present. To correct for these biased AOD values, a multiplication factor approach is used that accounts for the cirrus cloud contribution of the total measured transmittance [*Shiobara and Asano*, 1994; *Kinne et al*., 1997]. To summarize, the efforts of using Sun photometry measurements under cirrus are concentrated on derivation of correction factors for a better AOD estimation rather than on deriving the actual cirrus COT. Recent work by *Devore et al*. [2012] demonstrated the ability to derive cirrus properties from Sun and Aureole radiance Measurements with the SAM instrument. Since most of the ground-based Sun photometers deployed globally (e.g., AERONET) span only the visible (VIS) to near-infrared (NIR) spectral range from 380 to 1020 nm, where cloud optical thickness is wavelength invariant, little work has been done in terms of exploiting the spectral domain to actually infer COT or ice particle effective diameters (D_{eff}). Very recently, COT was derived from the AERONET station in Leipzig using the 1640 nm band filter [*Seifert et al*., 2011]. However, these retrieved values were not corrected for any of the aforementioned effects so that the retrieved COT values for this case were probably underestimated, as shown by *Devore et al*. [2012, Appendix] for the AERONET FOV, and could be smaller than the actual values by 10–250% depending on the ice cloud D_{eff}. It may be noted here that the recently published AERONET cloud product [*Chiu et al*., 2010] relates to zenith viewing radiance measurements that result in the retrieval of water cloud optical thicknesses using transmittance lookup tables derived for clouds containing spherical water droplets.

[5] In this work, we present a fresh look at the topic of cirrus property retrieval by Sun photometers and suggest a methodology to exploit the additional information content that lies within the forward scattered irradiance component measured by these instruments. We use the combination of this measure and multi/hyper-spectral capabilities over the VIS through shortwave infrared (SWIR) range from 400 to 2200 nm commonly used by many other cloud retrieval schemes [e.g., *Nakajima and King*, 1990] to demonstrate the retrieval feasibility of both cirrus COT and ice particle effective diameter by Sun photometry. Our approach is generalized to cover the full range from 400 to 2200 nm to allow the implementation of the method on multi-spectral filter-based instruments (such as AATS-14) [*Russell et al*., 1993] or hyperspectral sensors (4STAR—Spectrometer for Sky-Scanning, Sun-Tracking Atmospheric Research) [e.g., *Dunagan et al*., 2011; *Schmid et al*., 2011].

[6] We begin with a forward modeling approach that uses detailed, wavelength-dependent cirrus cloud optical properties and phase functions derived by *Baum et al*. [2005b, 2011] for a range of COT and D_{eff} values spanning the hyperspectral range of 400–2200 nm. With our modeled results, we construct spectrally dependent lookup tables (LUT) and show the applicability of shorter wavelength (VIS) and longer wavelength (SWIR) transmittance dual-wavelength plots in determining cirrus COT and D_{eff}. The choice of using a specific and optimized wavelength set is also discussed. Following this assessment, we test the applicability, accuracy, and constraints of this approach by comparing modeled irradiance values with a few selected measurements made by AATS-14 for an airborne case from the ARCTAS summer 2008 campaign and also for a high-altitude ground-based case using data collected at the Mauna Loa Observatory (MLO) in Hawaii. Comparison of the retrievals using two different cirrus optical property data sets, which represent smoothed and roughened particle models [*Baum et al*., 2011], and the inspection of climatological-specific cirrus optical property data sets, sheds some light on the needed accuracy of the phase functions in the forward-most scattering angles. Applicability for other Sun photometers and global implications are also discussed.

2. The Forward Modeling and Retrieval Approach

2.1. Modeling Apparent Transmittance When Cirrus Is Present

[7] The present approach simulates the total transmittance that reaches the Sun photometer FOV when tracking the Sun through a cirrus layer. The total irradiance seen by the detector consists of both the direct attenuated solar irradiance $I_{\mathrm{dir}}(\lambda)$ and a forward scattered irradiance component $I_{\mathrm{fs}}(\lambda)$ due to the cirrus layer. To calculate the total transmittance ($T(\lambda)_{\mathrm{tot}}$) that includes both the direct and forward scattered components, we use a function suggested by *Shiobara and Asano* [1994]. The wavelength-dependent total transmittance term, based on *Shiobara and Asano* [1994] is

$$T(\lambda)_{\mathrm{tot}} = e^{-}\left[k\tau_c(\lambda) + \tau_{O_3}(\lambda) + \tau_{\mathrm{NO_2}}(\lambda) + \tau_{\mathrm{H_2}O}(\lambda) + \tau_{O_2}(\lambda) + \tau_{O_4}(\lambda) + \tau_{\mathrm{CO_2}}(\lambda) + \tau_{\mathrm{CH_4}}(\lambda)\right]/\mu \quad (1)$$

where subscripts correspond to cloud, ozone, NO_2, water vapor, O_2, O_4 (oxygen dimer), CO_2, and CH_4 optical depths, respectively, μ is the cosine of the solar zenith angle (SZA), k is the cirrus scattering phase-function dependent pre-factor (defined below), and $\tau_c(\lambda)$ is the spectrally dependent cloud optical thickness (COT) calculated from

$$\tau_c(\lambda) = \tau_c(550\ \mathrm{nm})\frac{Q_{\mathrm{eff}}(\lambda)}{Q_{\mathrm{eff}(550\ \mathrm{nm})}} \quad (2)$$

where $Q_{\mathrm{eff}}(\lambda)$ is the wavelength-dependent cirrus extinction efficiency.

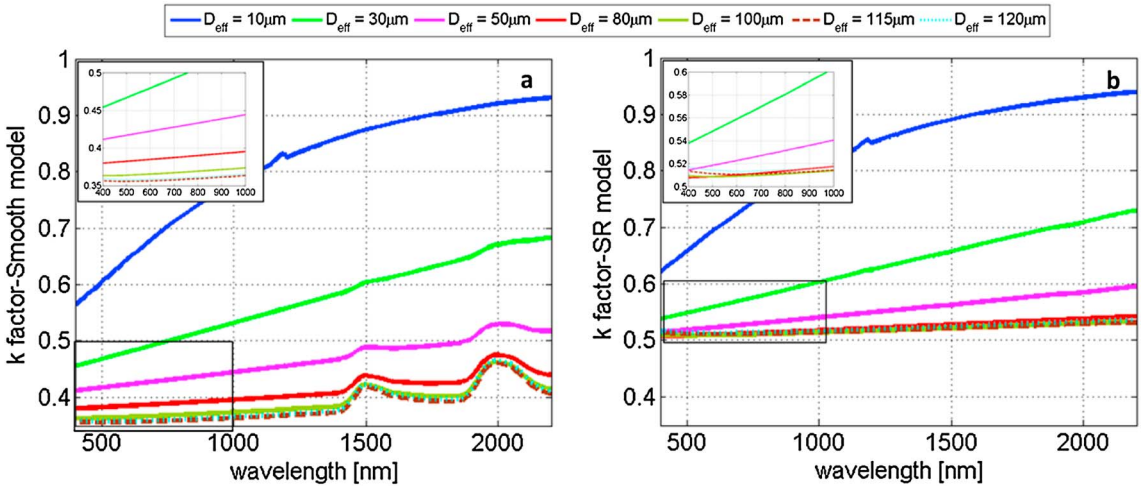

Figure 1. Cirrus scattering phase-function dependent pre-factor k (equation (3)) calculated at half-width FOV $\boldsymbol{\eta}$ of 1.85° for phase functions based on *Baum et al*. [2011] (a) smooth-faceted and (b) severely roughened (SR) ice crystal models. Different line colors correspond to the various ice crystal effective diameters shown. Insert expands the rectangular area marked in the lower left of each plot.

[8] *Shiobara and Asano* [1994] show that the pre-factor that best fits their Radiative Transfer (RT) Monte Carlo simulation results can be calculated using

$$k(\eta,\lambda,D_{\text{eff}}) = 1 - \varpi(\lambda,D_{\text{eff}})\frac{\int_0^{\eta} P(\theta,\lambda,D_{\text{eff}})\sin\theta d\theta}{2} \quad (3)$$

[9] Here, $\varpi(\lambda,D_{\text{eff}})$ is the wavelength-dependent single scattering albedo for the corresponding ice particle effective diameter (D_{eff}), $P(\theta,\lambda,D_{\text{eff}})$ is the ice cloud scattering phase-function (which is normalized to 2 and is both wavelength and ice effective diameter dependent), θ is the scattering angle, and η is the Sun photometer FOV half-angle. As an example, Shiobara and Asano show that for the smooth-faceted hexagonal ice particle scattering phase function of *Takano and Liou* [1989] at a wavelength of 550 nm and for a Sun photometer half-FOV of 1.2°, k calculated from equation (3) is 0.521. Our own calculations of k from equation (3) for the *Baum et al*. [2011] phase functions for smooth-faceted (hereafter Smooth model) and severely roughened (hereafter SR model) ice models at wavelengths spanning 400–2200 nm, and half-FOV η of 1.85° yield the values shown in Figures 1a and 1b, respectively. The D_{eff} is defined as 1.5 times the ratio of the total ice volume to its total projected area [*Baum et al*., 2005a]. It is interesting to note that for the large D_{eff} values (i.e., above 100 μm), the k values collapse to be almost the same in each of the models. Also, at 550 nm, k values are close to 0.51–0.52 (i.e., *Shiobara and Asano* [1994] values) for $D_{\text{eff}} < 30$ μm for the Smooth model and for diameters larger than 50 μm for the SR model. Both models show a general trend of slightly decreasing values from 400 nm toward 550 nm and increasing toward the longer wavelengths for the larger effective diameters (see figure inserts). At smaller D_{eff}, there is a strong monotonic increase of k values with wavelength for both models. This figure strongly demonstrates the variability in k values as a function of D_{eff} from the various ice cloud single-scattering models.

[10] Figure 2 provides the wavelength-dependent total transmittance (calculated by equation (1)), which includes both the direct attenuation effect and scattered light due to cloud and gases and the direct attenuated transmittance term alone (due to cloud and gases), calculated by equation (4):

$$T(\lambda)_{\text{direct}} = e^{-\left[\tau_c(\lambda)+\tau_{O_3}(\lambda)+\tau_{NO_2}(\lambda)+\tau_{H_2O}(\lambda)+\tau_{O_2}(\lambda)+\tau_{O_4}(\lambda)+\tau_{CO_2}(\lambda)+\tau_{CH_4}(\lambda)\right]/\mu} \quad (4)$$

[11] Rayleigh optical depth is not included in the model derivation or in the figure because it has a very strong wavelength dependency; this would have masked the cloud wavelength dependency component. Accordingly, it is also subtracted from the transmittance measurements shown later.

[12] Figure 2a shows the wavelength-dependent direct transmittance (calculated by equation (4)), for various COT values for $D_{\text{eff}} = 10$ μm (dotted lines) and $D_{\text{eff}} = 120$ μm (thick solid lines) for a SZA of 30°. Figure 2b shows the total transmittance term (calculated by equation (1)), which includes both the direct and scattered terms. Gaseous transmission terms are calculated with MODTRAN 5.2.1 version for a mid-latitude model atmosphere (columnar water vapor amount of 2.9225 g cm^{-2}). In general, the total transmittance values (Figure 2b), which represent the "apparent" transmittance seen by the detector, are higher than the direct transmittances for the corresponding COT values, as expected. The differences are seen both within the water vapor (e.g., 940, 1120 nm) absorbing bands and also in the atmospheric window regions. The transmittances (i.e., irradiances) look similar in shape but have higher values than the direct transmittance values (Figure 2a) for the large D_{eff} values. However, the transmittances show differences for the small D_{eff} values. This provides a hint for the possibility of inferring cloud D_{eff} from direct sun measurements. For a given COT, the separation between small and large D_{eff} decreases with increasing wavelength. This trend is different from the observed trend for diffuse transmittance calculations of water clouds [*McBride et al*., 2011], where at a given cloud optical thickness, there is a crossover at different cloud D_{eff} within the water absorption regions. In the Sun

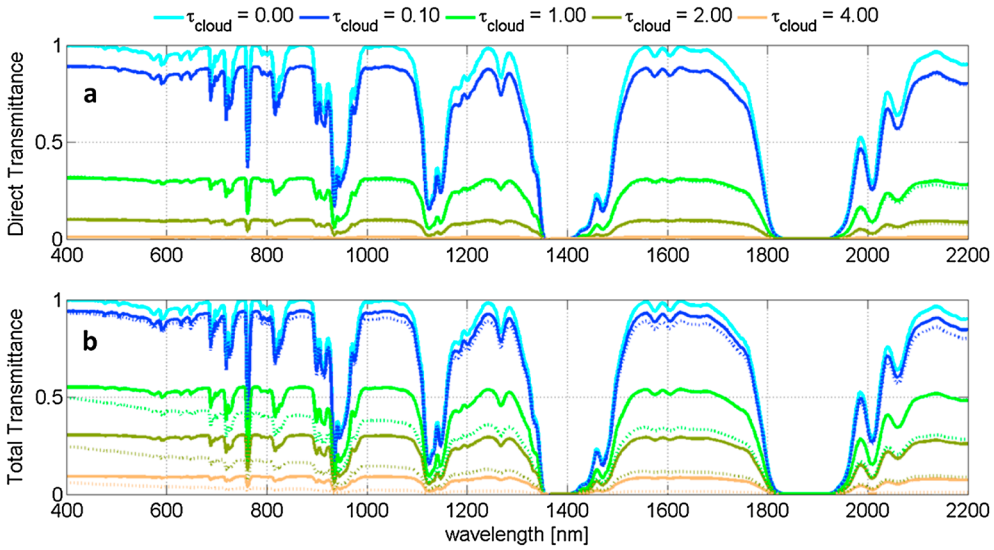

Figure 2. (a) Direct solar transmittance (equation (4)) calculated through a cirrus layer for a range of cloud optical depths (τ_{cloud}) and for cloud effective diameters of 10 μm (dotted lines) and 120 μm (thick solid lines) (calculations include the appropriate trace gas attenuation terms); and (b) corresponding values of total transmittance (equation (1)) calculated for a 1.85° half-width FOV for cloud effective diameters of 10 μm (dotted lines) and 120 μm (thick solid lines). Cirrus optical properties are taken from *Baum et al.* [2011] SR model. Calculations are made for a solar zenith angle (SZA) of 30° for the Mid-Latitude Summer atmosphere.

photometer case only the scattered light component affects the change in the observed spectra with regard to the additional information gained from it, and hence, the behavior is smooth with wavelength. Other model atmosphere simulations were made (1976 U.S. Standard and Tropical) and result in similar trends. The only noticeable difference is due to the various water vapor amounts for each model. For example, the tropical model simulations (columnar water vapor amount of 0.6 g cm^{-2} at an altitude of 3.4 km) yield higher transmittance values in the 1380 nm water vapor band. This band is of specific interest since it is used as the standard MODIS cirrus retrieval band [*Gao et al.*, 2004]. In contrast to the MODIS algorithm that uses a relatively high reflectance value to determine the presence of a cloud, the Sun photometer result does not show a unique behavior as the cirrus COT or Deff varies, and follows the same smooth wavelength-dependent behavior at all wavelengths.

[13] Figure 3 examines an example of dual-wavelength transmittance plots that are often used in the classic solar wavelength retrieval algorithms [e.g., *Nakajima and King*, 1990; *Platnick et al.*, 2003; *McBride et al.*, 2011] and are relevant for Sun photometers currently operating (e.g., 2138 nm for AATS-14 and 1640 nm for some of the AERONET instruments). As seen from Figure 3b, and from other cloud retrieval algorithms [e.g., *Nakajima and King*, 1990], it seems that only the combination of a VIS (i.e., not absorbing) wavelength with a SWIR wavelength beyond 1000 nm (slightly absorbing) would permit the inference of COT and D_{eff}. Some wavelength pairs show better separation potential than others because they span a larger domain on these dual-wavelength transmittance plots (e.g., Figures 3c and 3d versus 3f). In this work, we examine the use of more than two wavelengths in the overall retrieval scheme.

[14] To make our analysis more general, Figure 4 shows the calculation of the net transmittance signal gain (equation (1) minus equation (4)) for three different half-width FOV values that represent a range of current operational Sun photometers (1.85°, 1.0°, and 0.6°, representing AATS-14, 4STAR, and AERONET instruments, respectively). The results are computed for an optically thin cirrus layer with COT = 0.1 (Figure 4a), and for COT = 1 (Figure 4b). The latter represents the maximum signal gain possible based on similar calculations for the whole COT range. Dashed lines are for D_{eff} = 10 μm and solid lines are for D_{eff} = 120 μm. In general, larger particles "add" (scatter) more light into the instrument FOV than smaller particles, resulting in an increased signal, even for Sun photometers with a narrow FOV. Smaller particles, on the other hand, have a strong wavelength dependence that might allow a more unique and accurate retrieval, even for a relatively low signal. In general, decreasing FOV half-width sizes will reduce the signal, providing less information, which will probably lead to lower separation ability in the final retrieval procedure. This is in contrast to the common practice that aspires to minimize Sun photometer FOV to decrease possible bias effects from similar sources. Indeed, Sun photometers are not designed to measure scattered light, and their goal is to minimize this effect. Under specific conditions (such as tracking the Sun through a cirrus layer), a slightly larger FOV might be preferred for the inference of cirrus optical and microphysical parameters.

2.2. Cirrus Optical Property Models

[15] The bulk ice cloud optical properties (extinction efficiency, asymmetry parameter, single scattering albedo, and the scattering phase function) used in this work are taken from the past and present work published by *Baum et al.* [2005b, 2011]. These data sets are based on merging the most up-to-date ice particle scattering properties with a compilation of microphysical data from many field campaigns using measured particle distributions (1117 and 12,815

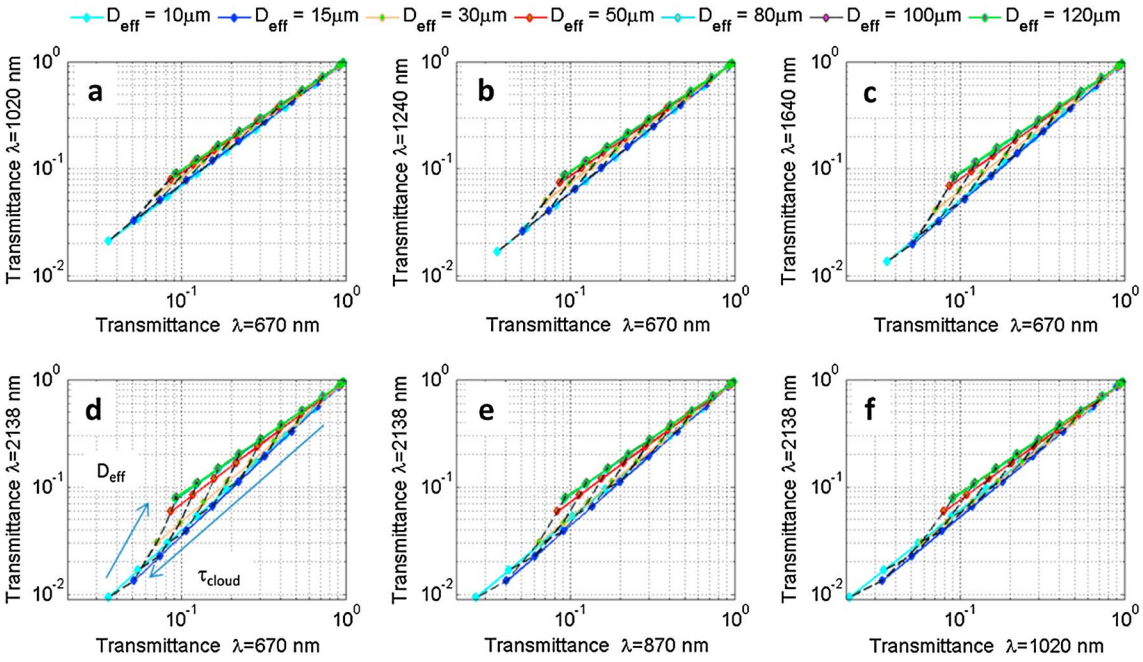

Figure 3. Total transmittance (equation (1)) calculated for the Mid-Latitude Summer atmosphere model at SZA of 30° at wavelengths (a) 1020 nm, (b) 1240 nm, (c) 1640 nm, (d) 2138 nm versus 670 nm, (e) 2138 versus 870 nm, and (f) 2138 versus 1020 nm for the *Baum et al*. [2011] SR optical properties data set. Arrows point in direction of increasing COT values (0–4) and D_{eff} values (10–120 μm).

particle size distributions for the 2005 data set [*Baum et al*., 2005b], and the recently published data set [*Baum et al*., 2011], respectively) with varying ice water content (IWC) values. The 2011 model includes the adoption of new ice habits (hollow bullet rosette and small/large aggregate of plates) and a treatment of ice particle surface roughening, with smooth particles having a roughness factor $\sigma = 0$ and severely roughened particles having $\sigma = 0.5$. The library of individual ice particle scattering properties is based on more accurate light scattering methods than the ones used for the older models [i.e., *Baum et al*., 2005b], which are used in the MODIS collection 5 cloud retrieval algorithm. The single scattering properties of the *Baum et al*. [2011] models incorporate a new habit mixture, which results in a continuous representation of the particle habit throughout the entire size distribution range provided by the microphysical data. The *Baum et al*. [2011] data set includes three primary models that represent ice cloud in situ measurements: The generalized habit mixture (GHM) is based on the full set of microphysical data from various midlatitude and tropical field campaigns, regardless of cloud temperature. The Mid-Latitude (MLT) mixture is based on data taken between −40°C and −60°C and has a higher fraction of solid and hollow bullet rosettes but excludes aggregates of plates

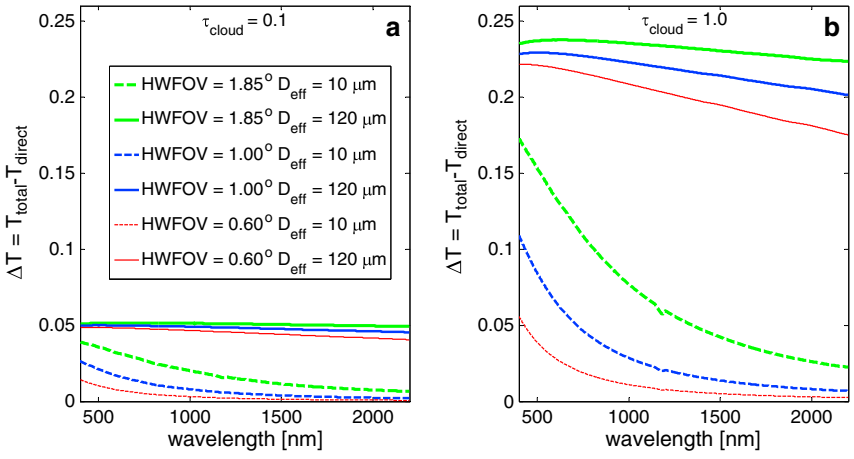

Figure 4. Net transmittance differences (equation (1) minus equation (4)) based on the *Baum et al*. [2011] SR model for three half-width FOV values (1.85°, 1.0°, and 0.6°, corresponding to the AATS-14, 4STAR, and AERONET Sun photometers, respectively) for a cirrus optical thickness (τ_{cloud}) of (a) 0.1 and (b) 1. Dashed lines are for ice particle effective diameter of 10 μm, and solid lines are for ice particle effective diameter of 120 μm.

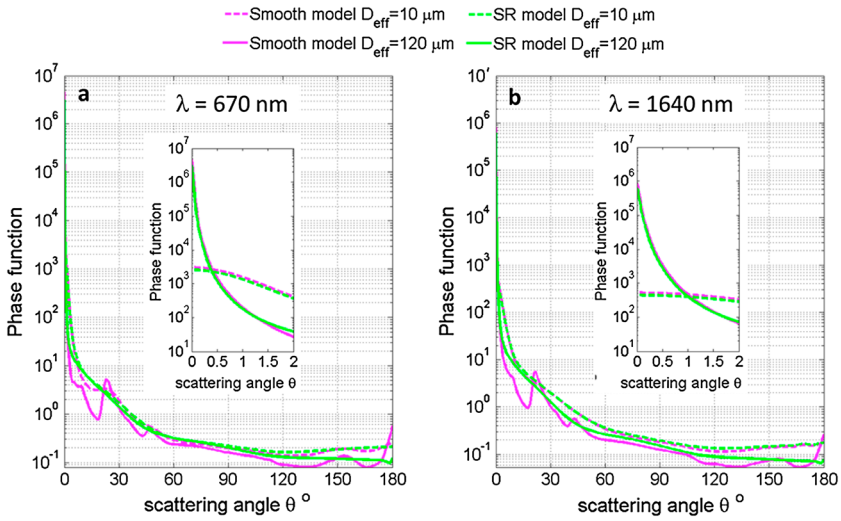

Figure 5. (a) *Baum et al*. [2011] smooth-faceted ice crystal model (magenta) and SR ice crystal model (green) scattering phase functions for the 670 nm visible band, and (b) same as Figure 5a but for the 1640 nm SWIR band. Dashed lines represent ice effective particle diameter of 10 μm, and solid lines represent ice effective particle diameter of 120 μm. Insert shows the first 2° of the scattering phase function.

because they are found primarily in anvils associated with deep tropical convection. Finally, the Tropical Deep Convective (TDC) model excludes droxtals and relies heavily on aggregates of plates as one of the major habits in this mixture. All three sets of models assume that the ice particles are severely roughened ($\sigma = 0.5$).

[16] Ice particle surface roughness is found to improve the agreement between modeled and measured backscattering phase matrix components measured by CALIOP [*Baum et al*., 2011]. Additionally, the ice models based on the GHM and severe roughening improved the agreement with PARASOL (Polarization and Anisotropy of Reflectances for Atmospheric Sciences coupled with Observations from a Lidar) polarized reflectance data as shown in *Cole et al*. [2013]. For the ensuing analysis, we adopt the general habit mixture (GHM) model [*Baum et al*., 2011] assuming severely roughened particles (SR model) or smooth-faceted particles (Smlooth model). This model was chosen because it is the most general ice cloud bulk optical model and is the extension of the 2005 model [i.e., *Baum et al*., 2005b]. The latter is used in the MODIS operational collection 5 cloud retrieval algorithm, in the suggested MISR thin cirrus retrieval algorithm [*Pierce et al*., 2010] and in a recent study on retrieving cirrus properties using Sun Aureole Measurement (SAM) instrument by *DeVore et al*. [2012]. The 2005 model was derived using the assumption of smooth ice particle surfaces ($\sigma = 0$) for all habits except the aggregate of solid columns for which severe roughening was adopted. The new 2011 Smooth model is different from the latter through the inclusion of new habits and the adoption of the general habit mixture recipe.

[17] The 2011 ice cloud bulk optical property models (both Smooth and SR) encompass values of the effective diameters from 10 to 120 μm in increments of 5 μm. This smaller range of effective diameter (in contrast to 10–180μm for the *Baum et al*. [2005b] models) was the result of limiting the microphysical data to ice cloud measurements for which the temperature was less than −40°C, while the earlier models included data at $T \leq -25$°C. The effect of this is to decrease the data from clouds with higher IWC that tend to have higher D_{eff} values. Moreover MODIS collection 5 retrievals tend to fall within the range between 30 and 70 μm, with decreasing sensitivity to large particles. Optical properties are provided for the spectral range of 400–2200 nm, with a resolution of 10 nm. The difference between the 2011 Smooth and SR models can be seen in Figure 5 for two distinct wavelength regions (the 670 nm VIS band and the 1640 nm SWIR band). This figure shows the angle-dependent phase function for two D_{eff} sizes (i.e., 10 and 120 μm) for the two models. The inclusion of severe particle roughening tends to smooth out the maxima in the phase functions so that there are no halos at scattering angles of 22° and 46° for the larger effective diameters, and backscattering is greatly reduced over that in the smooth particle models. The general separation ability due to different intensities of the small and large effective diameters, at angles close to 180° decreases in the 2011 SR model. This is in contrast to the trend observed in the Smooth model. The latter effect may be of future importance for the attempted cirrus retrievals from multi-angular sensors such as the one that was recently investigated with the MISR satellite [*Pierce et al*., 2010], which used the Smooth-ice faceted model [*Baum et al*., 2005b]. Nevertheless, at forward scattering angles, the intensities of the phase function for the two effective diameters remain fairly unchanged in shape but differ slightly in intensity (note the logarithmic scale) as shown in the insets of the two main panels of Figure 5. Figure 6 emphasizes further the difference between the Smooth and SR phase functions. The Smooth model spans a smaller domain in the 670–2138 nm transmission dual-wavelength calculations. From the figure, we can estimate that the retrieved COT would be higher and D_{eff} would be higher for the same data point with the Smooth model.

[18] Given the choice in the GHM model (with Smooth and SR parameterization) as the primary model for our analysis, it is instructive to investigate further the difference of the forward scattered peak with the other available cirrus models. In addition to the MLT and TDC mixed habit

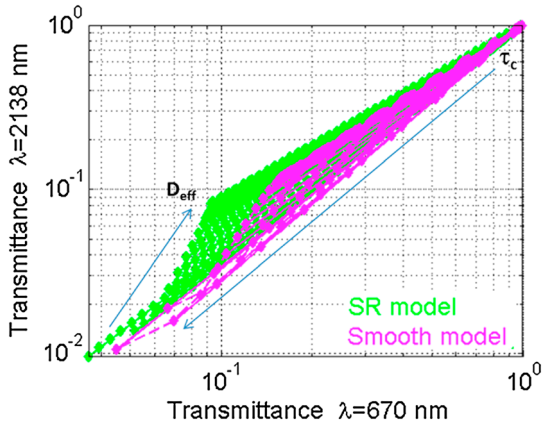

Figure 6. Dual-wavelength transmittance lookup table values for *Baum et al.* [2011] Smooth (magenta) and SR (green) models. Values are calculated for SZA of 30°. Arrows point in direction of increasing values of COT (τ_c from 0 to 4) and ice particle effective diameters (D_{eff} from 10 to 120 μm).

models, a single habit model based on the severely roughened aggregate of solid columns (ASC) is also adopted. Of the nine ice habits used in the mixed recipe models, the severely roughened ASC has two unique properties: (a) the asymmetry parameter is much lower than that of the other habits and (b) the asymmetry parameter is fairly independent of particle size, ranging from 0.75 to 0.76 at a visible wavelength of 650 nm. All other models exhibit an increase in the asymmetry parameter with wavelength and with particle effective diameter (about 0.8 at 650 nm and between 0.8 and 0.9 at 1650 nm). Because the asymmetry parameter of the severely roughened ASC model is also much lower than those values currently used for MODIS collection 5 retrievals (based on smooth particles), adoption of this particle model is expected to result in lower inferred optical thicknesses and larger ice particle effective diameter sizes [*Baum et al.*, 2011], thereby reducing the differences between MODIS retrievals based on solar bands, infrared (IR) window bands, and also CALIPSO/CALIOP retrievals [*Garnier et al.*, 2012]. However, the severely roughened ASC model has some deficiencies, being a very dense particle with a high volume to area ratio (which defines the effective diameter), thereby resulting in higher calculated ice water content values relative to in situ measurements for a given particle size distribution. Additionally, the polarization properties of this habit do not match well with PARASOL measurements [*Cole et al.*, 2013].

[19] Figure 7 illustrates the different phase functions for the above models. Figures 7a–7c show the entire scattering angle range and Figures 7d–7f show only the most forward 2° of the phase function; the forward scattering angles are used in the Sun photometer retrieval. The relative intensity differences are rather small at the 180° backscattering angle for all models. This feature probably translates into the relatively lower sensitivity in the retrieval procedure looking at the angles closest to 180° [*Baum et al.*, 2011]. At the forward scattering angles, within 2°, there are somewhat larger differences between the various habit models (all models shown in Figure 7 are parameterized as severely roughened). The MLT model shows the lowest intensity values at all effective diameters. In contrast, the ASC has the highest intensity values, especially for smaller effective particle diameters. We note that this aggregate particle was intended for use in representing the largest particles in a particle size distribution, not the smallest particles in a distribution. In view of these observations, we reconstruct the transmittance LUT (similar to those shown in Figure 3) for the MLT, TDC, and ASC models for further investigation. A comparison of the LUTs indicates that there is less variation among the mixed habit models themselves than between the mixed habit models and the severe roughened ASC model. It should be noted that in practice, the TDC model is a less likely candidate for measurements by Sun photometers due to the relatively large optical thickness of deep convective ice clouds and their anvils (i.e., exceeding a COT of 4), which limit the direct sunlight able to penetrate through the cloud. Following this, LUTs for the MLT and ASC models are used below in retrieving cirrus properties from the ARCTAS case, and the results and implications are then discussed.

2.3. The Retrieval Scheme

[20] The retrieval is based on the lookup table (LUT) approach, in which calculations are performed that span COT values from 0 to 4 in increments of 0.02 from 0 to 1 and increments of 0.1 from 1 to 4. This results in the LUT being defined at 81 COT values. D_{eff} values are used at the same nominal values (i.e., 23 values) given by *Baum et al.* [2011] without interpolation. Spectrally dependent transmittance values are calculated for the range of 400–2200 nm using the wavelength-dependent values in the cloud optical property database [*Baum et al.*, 2011]. These are interpolated on a high-resolution wavelength grid (i.e., 0.2 nm), which allows the appropriate convolution of results with the specific instrument filter (or slit) functions.

[21] The LUTs are calculated for each retrieval point (i.e., measured transmittance data point that is identified as cloud flagged), accounting for the SZA at the corresponding time of measurement, and the atmospheric pressure and instrument altitude (when airborne or ground-based). The model includes the range of COT and D_{eff} values mentioned above, but excludes the Rayleigh scattering contribution. Gas transmittance is calculated using MODTRAN simulations in direct transmittance mode (e.g., using the Mid-Latitude Summer atmosphere for the ARCTAS case and the Tropical atmosphere model for the MLO case), accounting for SZA and instrument altitude for each data point. The measured total transmittances are corrected for the Rayleigh slant transmission calculated for the corresponding instrument pressure and time of day. The retrieval is performed by minimizing the chi-square measure defined as

$$\chi^2 = \sum_{i=1}^{n} \left(\frac{y_{\mathrm{meas},i} - y_{\mathrm{mod},i}}{y_{\mathrm{mod},i}} \right)^2 \quad (5)$$

where $y_{\mathrm{meas},i}$ and $y_{\mathrm{mod},i}$ are the measured and modeled transmittance values, respectively, at a specific wavelength i. In this case, each wavelength is weighted equally. In the results section we demonstrate the effect of using different wavelengths sets in the retrieval. The retrieval uncertainty accounts for the uncertainty in each of the bands. This is estimated through the propagation of the retrieval fitting procedure on a perturbed measured transmittance (i.e.,

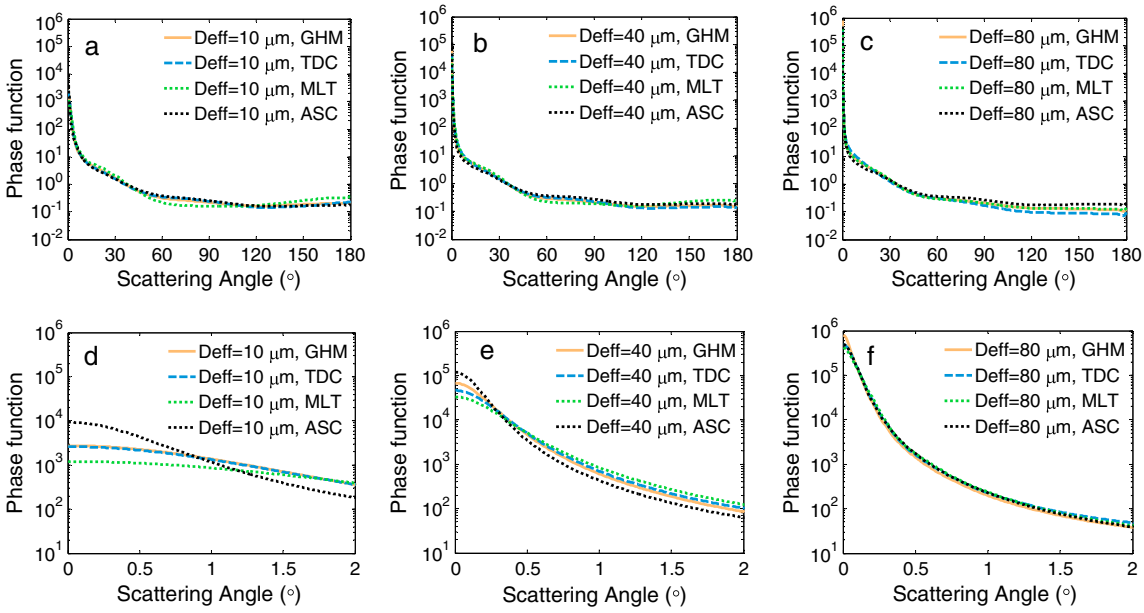

Figure 7. Phase functions for full range of scattering angles for the General Habit mixture (GHM), Tropical Deep Convective (TDC), Mid-Latitude (MLT), and aggregate of Solid columns (ASC) cirrus cloud models of *Baum et al.* [2011] at a wavelength of 650 nm for ice crystal effective diameter of (a) 10 μm, (b) 40 μm, and (c) 80 μm; and (d–f) phase functions for 0–2° forward scattering angles for Figures 7a–7c. All models shown have severe roughened parameterization (i.e., $\sigma = 0.5$).

$y_{\mathrm{meas},i} \pm \sigma_i$). Then, the delta of the retrieved values from the perturbed transmittance are added or subtracted from the actual retrieved values to obtain retrieval error-bars. Transmittance uncertainty estimation for each of the AATS-14 bands (σ_i) is described in section 3.1.

2.4. Modeling Apparent Transmittance Under a Mixed Layer of Aerosols and Cirrus

[22] Although airborne Sun photometry platforms can make high altitude measurements of cirrus, and thus avoid the majority of the atmospheric column aerosol contribution, under very thin cirrus the effect of even a small aerosol layer may be important. This may be further enhanced at locations where the background conditions are not pristine, and so even higher altitude measurements can be affected by the lower altitude aerosols that are transported to higher altitudes (e.g., biomass burning events as occurred during the ARCTAS 2008 summer campaign). In Figure 8, typical transmittance values are shown at two selected wavelengths (i.e., VIS and SWIR) for four modeled aerosol types, which include an absorbing case (i.e., urban), non-absorbing cases (i.e., clean marine and tropical marine), and desert dust. The solid black lines represent the corresponding transmittance LUT values based on the SR cirrus optical property model.

[23] Aerosol transmittance values are calculated based on the direct transmittance term in equation (4), replacing the wavelength-dependent COT term with an analogous one for aerosol values. The wavelength-dependent aerosol optical thickness for each of the models is calculated using the OPAC software package [*Hess et al.*, 1998], for the corresponding aerosol models. Transmittance values are calculated for a range of AOD values (τ_{aerosol}) of 0.01–4. Values of relative humidity (RH) are varied for the urban and marine aerosol type cases, as shown in Figure 8. Inclusion of only the direct term in the transmittance calculation for the aerosol models is justified due to the negligible amount of forward scattered light (less than 1%) for most types of aerosols [*Russell et al.*, 2004]. With dust, however, this may not be valid, and one should use an additional forward scattered contribution on the order of 5% at 675 nm, and less than 1% at wavelengths beyond 1500 nm for the AATS FOV [*Russell et al.*, 2004]. These calculations are used to determine how results from the different aerosol models compare to those from the cirrus transmittance model at the various wavelengths. Figure 8 shows that most aerosol types are well separated from the cirrus. VIS transmittances due to aerosol extinction alone are less than for the corresponding COT. This might permit the separation of cirrus cases from aerosol cases. We note that this separation under cirrus will be more challenging when dust particles are present, as was also shown recently with the MISR cirrus retrieval algorithm [*Pierce et al.*, 2010]. In the present case, we investigate the effect of absorbing (i.e., biomass burning) and pristine (i.e., marine tropical) aerosol types on our measurements and hence, do not attempt to develop a more detailed scheme for the dust case at this time.

[24] Figure 9 examines the effect of mixed aerosol and cirrus layers. The aerosol model that is chosen for the illustration is the absorbing type (OPAC urban model, which includes a mixture of mainly soot and water soluble components). We construct four mixture cases (i.e., two component model), using values of 0.01, 0.05, 0.1, and 1.0 for aerosol optical depths, together with the cirrus model that is calculated for a range of cloud optical thicknesses of 0–4. As shown, aerosol optical depths >0.01 can affect the total transmittance values (depending, of course on the specific aerosol optical properties). Specifically, the addition of aerosols acts to reduce VIS transmittance values. A larger effect is seen within the relatively low cirrus optical thicknesses

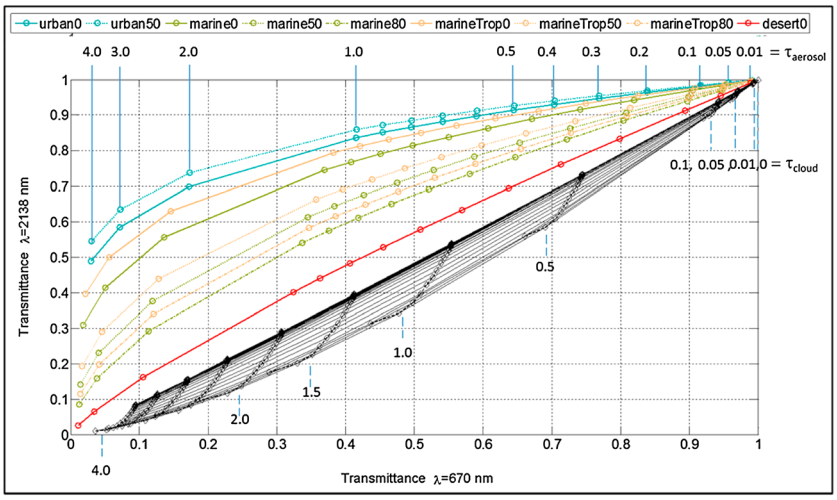

Figure 8. Modeled direct transmittance of various aerosol models from the OPAC database at various aerosol optical depths (0.01–4) for SZA of 30°. Aerosol models correspond to urban (at 0% and 50% RH), clean marine (at 0%, 50%, and 80% RH), tropical marine (at 0%, 50%, and 80% RH), and desert dust models. Solid black lines represent the modeled total transmittance using equation (1) at various cirrus optical thicknesses (0–4).

(upper right portion of the figure). In the results section, we examine this effect for a sample case from the ARCTAS 2008 summer campaign.

3. Results and Discussion—Implementation of the New Approach on Sample Cases

3.1. Data Analysis

[25] Two case studies using the AATS-14 measurements are chosen (i.e., ARCTAS 9 July 2008 and MLO 29 September 2011) to demonstrate our approach. The general retrieval scheme is described in section 2.2 and here we address the specific retrieval implemented for the AATS-14 Sun photometer.

[26] Data points for the cirrus properties retrieval are chosen according to a sequence of pre-processing steps as follows:

[27] 1. A pre-determined relative standard deviation value (e.g., 1%) is adopted for a typical measurement period of 3 s (and a sample rate of 3Hz), where measurements above this value are classified as cloud-contaminated.

[28] 2. Standard retrieved wavelength-dependent AOD values for the AATS-14 instrument are used to set an additional cloud screening threshold.

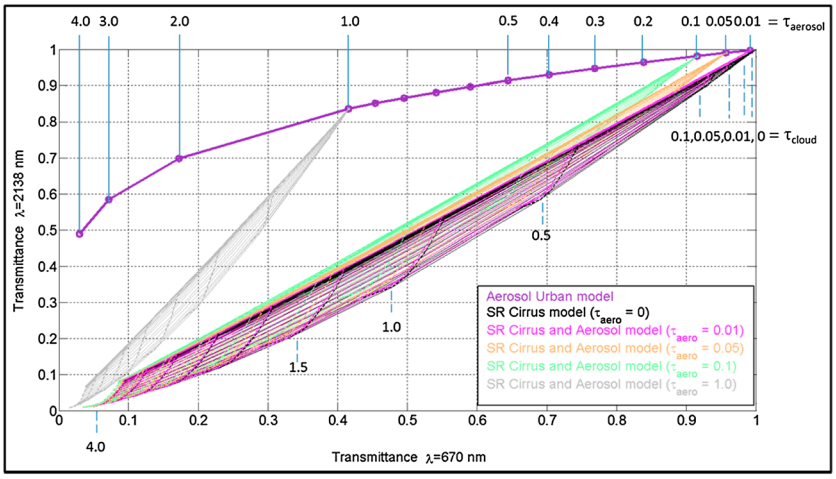

Figure 9. Modeled total transmittance for a two component cirrus (SR model) plus aerosol model using the OPAC urban aerosol model (0% RH) for four values of AOD (values listed correspond to the value at 550 nm, but AOD was varied with wavelength according to the extinction wavelength-dependent function for the urban aerosol model, as detailed in text). Solid purple line represents the modeled direct transmittance due only to the direct aerosol extinction, at solar zenith angle of 30°. Cirrus model values are based on *Baum et al*. [2011] SR data set and are shown as gridded lines, colored according to amount of aerosols in the two-component model.

[29] This threshold is based on a second order polynomial fit to the wavelength-dependent retrieved AOD values:

$$\ln(\tau_{\text{aero}}(\lambda)) = a_0 + a_1 \ln(\lambda) + a_2 \ln^2(\lambda) \quad (6)$$

where τ_{aero} is the wavelength-dependent (λ) measured aerosol optical depth and a_0, a_1, and a_2 are the second-order polynomial fit parameters that best match the measurements. The parameter a_1 provides a useful measure of the AOD wavelength dependence and equals the traditional Ångström exponent for an AOD spectrum with $a_2 = 0$. Any data point below a fixed a_1 value, which is set according to the specific statistics of such values for a given data set, is also considered as cloud contaminated. This is based on the fact that clouds exhibit relatively weak wavelength dependence, especially up to 1000 nm. Threshold a_1 values that represent cloudy measurements for the ARCTAS case were determined as 0.5 above an aircraft (i.e., instrument) altitude of 4 km above sea level (ASL). This altitude is chosen based on HSRL (High Spectral Resolution Lidar) curtain plots [*Hair et al*., 2008] (for 9 July 2008), which showed that the most dense smoke plume was below 4 km (~3km above ground level), and on the instrument's operator notes regarding cirrus above the aircraft.

[30] The high spectral resolution modeled values (from equation (1)) are convolved with the specific AATS-14 filter response functions for each of the bands between 400 and 2200 nm. Filter full widths at half-maximum (FWHM) are ~5 nm, except for the 354 and 2138 nm channels, which have FWHM 2 and 17 nm, respectively. The minimization is conducted for three separate wavelength sets to assess the effect of the wavelength choice on the retrieval results. The first set (hereafter nine-wavelength case) includes the following nominal AATS center value bands: 499, 520, 605, 675, 779, 864, 1020, 1558, and 2138 nm. The second set (hereafter six-wavelength case) includes all wavelengths at and above 675 nm, excluding the strong ozone absorption and absorbing aerosols region (below 675 nm), and the third set included only two wavelengths (675 nm and 2138 nm) to compare with standard retrieval methods. The 451 nm and the 1240 nm bands are excluded due to inaccurate response function representation at the time of measurements, and the 940 nm band is excluded due to the high absorption of water vapor within this channel. The two shorter wavelength filters of the instrument (i.e., 354 and 380 nm) are excluded due to lack of optical property data for this region.

[31] Retrieval uncertainties are estimated by running the retrieval three times for each data point: for the measured transmittance, and for the measured transmittance plus or minus its uncertainty (i.e., $y_{\text{meas},i} \pm \sigma_i$). The differences between these retrieval results are translated into the retrieval error bars. Filter uncertainties σ_i are derived for each wavelength by taking the root sum square of the following error elements: the instrument calibration values (i.e., V_o, which is derived using the Langley method), the standard deviation measure of the voltage V, and the tracking error (which varies for each of the filters and corresponds to their FOV slope). These are relative values, which are then multiplied by the total measured transmittance to give absolute uncertainties. A more detailed description on the derivation of uncertainty measures for AATS-14 can be found in *Russell et al*. [1993]. Retrievals are made for both the Smooth and the SR models to test the sensitivity of the retrieved properties to the a priori assumed models. Also, a comparison among the three different wavelength sets and among the GHM, MLT, and ASC models is made for the ARCTAS case.

3.2. ARCTAS—9 July 2008—Airborne Case

[32] The ARCTAS mission (Arctic Research of the Composition of the Troposphere from Aircraft and Satellites) was conducted in two 3 week deployments based in Alaska (April 2008) and western Canada (June–July 2008). Its goal was to better understand the factors driving current changes in Arctic atmospheric composition and climate [*Jacob et al*., 2010]. Initial results from AATS-14 in ARCTAS are presented in *Shinozuka et al*. [2011] and *Shinozuka and Redemann* [2011].

[33] The sample case analyzed here is taken from the 9 July 2008 flight with the NASA P-3B aircraft. This flight sampled many smoke layers below or above low-level cumulus clouds and several cases of cirrus above smoke and cumulus clouds. Figure 10 shows all measurements for that day on a dual-wavelength transmittance plot. Data points are divided into sections of low (below 4km) and high (above 4km) aircraft altitudes. This altitude is chosen to be above most of the dense smoke layers and scattered low-level water clouds. Data are marked to show if they are identified as cloud instances (cloud flagged) or as clear sky aerosol instances (aerosol flagged). As expected, cloud-flagged data are prevalent in the plot. The high altitude (>4 km) threshold provides a better separation of the cases where cirrus observations are probably less affected by low clouds or dense smoke layers between the cirrus and the instrument. The choice of cloud-flagged data points above 4 km uses careful filtering and also confirmation with the instrument's operator flight notes. Nevertheless, they may contain unavoidable multilayered cloud scenes. As seen in Figure 10, most of the high altitude (>4 km) cloud-flagged data points (cyan circles) fall within the modeled dual-wavelength transmittance LUT domain in the figure (black shaded area). Some of the data, however, fall outside this LUT boundary. This is due in part to the fact that the plotted values are generated for a specific SZA of 45° and are shown at only two wavelengths. As will be shown later, the existence of an aerosol layer between the instrument and the cloud also affects the transmittance LUT values. Some low clouds do have lower transmittance values in the lower left part of the plot, which represents high COT (~3–4). However, since the low altitude cases might contain both cirrus and cumulus, together with smoke, they were conservatively filtered out and are not included in the analyzed data for the current case.

[34] A sample LUT of a two component model, consisting of the cirrus SR model and the ARCTAS smoke aerosol model (light brown solid line) for a constant AOD value of 0.05 at 550 nm is shown as the light brown shaded area in the figure. The OPAC Urban (purple solid line) and ARCTAS smoke models are clearly different; ARCTAS smoke has higher transmittance values at 2138 nm, which agrees better with the measured AOD data shown as orange circles in the figure. The two-component LUT results in almost the same LUT for both the ARCTAS smoke and the Urban aerosol models although a bit lower in visible transmittance values for the two component SR and ARCTAS smoke model. Hence, the two-component LUT using the OPAC Urban model and cirrus model is not shown

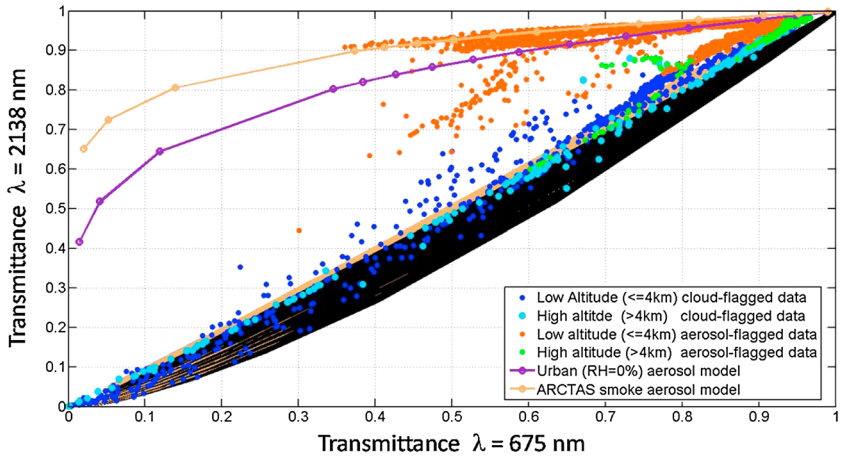

Figure 10. The AATS-14 measured transmittance values from ARCTAS 9 July 2008 case: low altitude (≤4 km) cloud-flagged data points (blue solid circles), high altitude (>4 km) cloud-flagged data points (cyan solid circles), low altitude (≤4 km) clear sky aerosol-flagged data points (solid orange circles), and high altitude (>4 km) clear sky aerosol-flagged data points (solid green circles). Solid purple line represents the modeled direct transmittance for the OPAC urban aerosol model (RH = 0%). Solid light brown line represents the modeled direct transmittance for ARCTAS smoke aerosol model, as detailed in text. Black shaded area represents calculated transmittance lookup table for a pure cirrus model, based on *Baum et al*. [2011] SR model, for a solar zenith angle of 45°, and is convolved with the corresponding AATS filter response functions. Light brown shaded area represents modeled transmittance lookup tables for the two-component model of the SR cirrus model with ARCTAS smoke aerosol model for AOD of 0.05 (at 550 nm).

in the figure. The average smoke aerosol wavelength-dependent optical depth is extracted from clear-sky smoke measurements for that day, and has an a_1 value of 0.94 ± 0.05, which is higher than the corresponding OPAC Urban model with a_1 value of 0.78.

[35] The ARCTAS smoke aerosol model is constructed from the measured AODs of smoke plumes under clear sky conditions. In particular, the measured average wavelength-dependent AOD spectrum is used to derive the corresponding factors that are needed for the extrapolation of the data to a range of optical depths spanning 0.01–4, as in the calculated OPAC models shown in Figure 8. From the average wavelength-dependent AOD values, we construct a multiplication factor based on the relation $Q(\lambda)_{\text{eff}}/Q(550\text{ nm})_{\text{eff}}$, which is introduced in equation (2), where τ_c is replaced here by τ_{aerosol} and the extinction efficiency ratio relates to the extinction efficiency of the appropriate aerosol model (from OPAC). This multiplication factor is derived by dividing the average AOD value at a specific wavelength by the corresponding one at 550 nm. To reconstruct the wavelength-dependent aerosol optical depth (τ_{aerosol}) for values in the range of 0.01–4, equation (2) is used with the derived multiplication factor instead of the explicit extinction efficiency value. We observe in Figure 10 that some of the high altitude cloud-flagged data fit better to the two component model (light brown shaded area). The highest deviation of the measured data from the "pure" cirrus case (black shaded area) occurs at COT values below 0.5. This result suggests that when very thin cirrus layers are present, the aerosol effect may be important and should be taken into account by the retrieval scheme.

[36] Cloud-flagged data points are processed to retrieve cloud products (i.e., COT and D_{eff}) using the Smooth and SR models. A two-component model that includes the cirrus model (Smooth or SR) and the ARCTAS smoke aerosol model (with a constant AOD value of 0.05) is also used in the retrieval scheme to test the effect of an aerosol layer below the cloud on the retrieval results and fit. This AOD layer value is estimated from clear-sky measurements above 4 km with AOD values between 0.01 and 0.1. By using a fixed AOD value, the aerosol layer between the instrument and the cloud is assumed to be constant, which may not be an optimal assumption. Nevertheless, this value is relatively small compared to the total cloud and aerosol layer and is used to demonstrate the importance of aerosols in our retrieval scheme. In Figure 11, retrieval results are filtered using a chi-squared threshold less than 0.001 and COT greater than 0.01. The error bars shown in Figure 11b are generated from the uncertainty retrieval runs as detailed above. The difference between the perturbed transmittance retrievals and the measured transmittance retrieval values is translated into the effective particle diameter error-bars. These error bars are not symmetric due to the nonlinear nature of the LUT. That is, underestimated transmittance values do not yield the same retrieval results as overestimated transmittance values. The uncertainties in the measured transmittance seem to have a negligible effect on the retrieved COT values, and hence error bars are excluded from Figure 11a.

[37] Table 1 summarizes COT and D_{eff} results for the various models and retrievals, including retrievals using Smooth and SR models, with or without an aerosol smoke model and results from using different wavelength sets in the retrieval and MLT and ASC models. The Smooth model (pure cirrus or with smoke) yields fewer valid retrievals compared to the SR model (pure or with smoke, respectively). We note that retrievals with the Smooth model yield valid results only for COT smaller than 0.8, although these retrievals produce slightly higher COT than do the corresponding

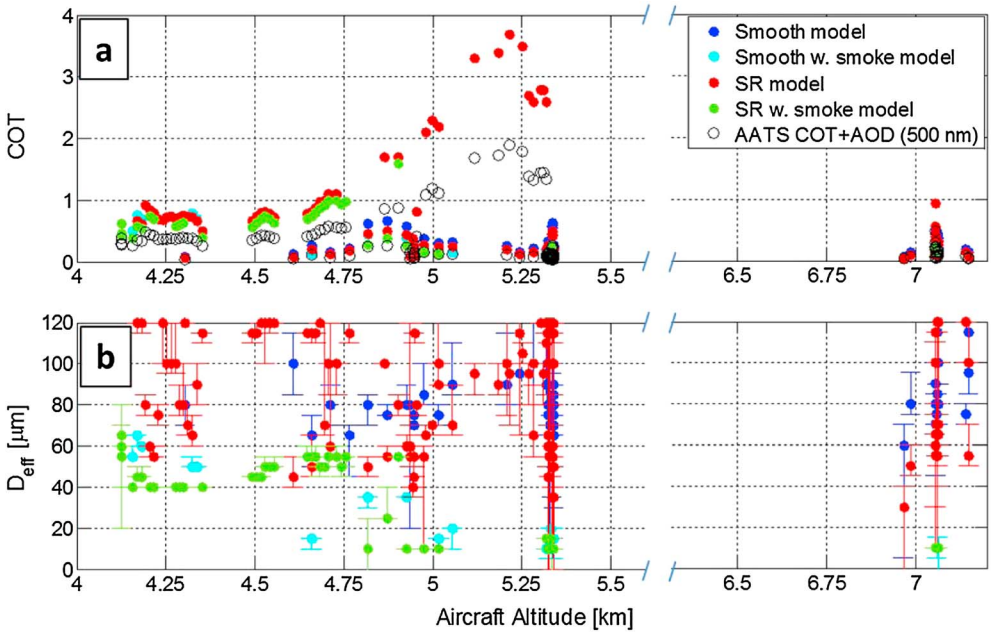

Figure 11. For 9 July 2008 ARCTAS case, valid retrieval values of (a) cirrus optical depth for the *Baum et al*. [2011] Smooth model (solid blue circles), *Baum et al*. [2011] SR model (solid red circles), a two-component model including the Smooth model and the ARCTAS smoke aerosol model with constant AOD value of 0.05 (solid cyan circles), a two-component model including SR model and the ARCTAS smoke aerosol model with constant AOD value of 0.05 (solid green circles), and AATS total retrieved optical depth (which includes both COT and AOD at $\lambda = 500$ nm) for the corresponding cloud-flagged cases (open black circles); and (b) corresponding ice particle effective diameter values for the models shown in Figure 11a. All retrieved data points are shown as a function of aircraft (i.e., AATS) altitude (ASL) and represent a total column quantity above the aircraft.

retrievals that use the SR model (Figure 11a and median values in Table 1). The difference between valid COT results for retrievals that use pure Smooth/SR models and corresponding valid COT results for retrievals that use Smooth/SR models with smoke is small. This is not the case for retrieved ice particle effective diameter, as shown in Figure 11b.

[38] The AATS-retrieved COT + AOD (at $\lambda = 500$ nm band) values are shown as open black circles in Figure 11a. These values are the result of using the standard AATS retrieval algorithm on the cloud-flagged points without any correction. As expected, they are lower than the COT values retrieved using the method introduced in this paper. This may be due in part to the overestimation in measured transmittance caused by ice particles scattering more light into the sensor, which results in an underestimation of the total optical depth. We also observe this trend at longer wavelengths (i.e., 1558 and 2138 nm, not shown in figure).

[39] It is interesting to examine the ratio between the retrieved COT using our proposed method and the standard retrieved AATS COT + AOD shown in Figure 11a. This ratio translates into a correction factor that might be used to correct Sun photometer COT + AOD values when cirrus is

Table 1. Summary Statistics for the ARCTAS Case Retrievals Using the Different Models

Model Used in Retrieval[a]	Valid retrievals (#)	COT[b]	D_{eff} [μm][c]	Retrieved COT/AATS(COT + AOD)
Smooth	88	0.06–0.66 (0.20)	50–115 (80)	1.65–2.50
Smooth w. smoke	25	0.06–0.78 (0.14)	10–65 (15)	0.69–2.10
SR (9w)	160	0.04–3.70 (0.18)	30–120 (100)	1.13–1.97
SR w. smoke (9w)	44	0.10–1.60 (0.57)	10–65 (40)	0.87–1.82
SR (6w)	153	0.04–3.70 (0.18)	30–120 (95)	1.10–1.97
SR w. smoke (6w)	45	0.04–3.50 (0.22)	35–115 (100)	1.10–1.96
SR (2w)	156	0.04–3.70 (0.18)	30–120 (85)	1.13–1.97
SR w. smoke (2w)	84	0.04–3.70 (0.18)	25–115 (75)	1.10–1.96
MLT	156	0.04–3.70 (0.18)	40–120 (120)	1.13–1.96
MLT w. smoke	46	0.08–1.00 (0.55)	10–85 (55)	0.73–1.76
ASC	149	0.04–3.70 (0.16)	10–120 (95)	1.10–1.96
ASC w. smoke	35	0.38–1.00 (0.56)	10–85 (30)	1.25–1.76

[a]GHM model is represented here by Smooth and SR models by *Baum et al*. [2011], both MLT and ASC models are used here only with the severe roughened parameterization (i.e., $\sigma = 0.5$). 9w, 6w, and 2w correspond to nine wavelengths, six wavelengths, and two wavelengths retrieval schemes, as detailed in text.
[b]COT-retrieved values are given as range (min-max). Values in parenthesis are the median values.
[c]Ice particle effective diameter retrieved values are given as range (min-max). Values in parenthesis are the median values.

present. As seen in Table 1, these values span a relatively large range that makes it difficult to translate this into a simple correction scheme. The Smooth cirrus model results in larger ratio values for the matching valid retrievals when compared to the SR model (see also median COT values in Table 1). Also, as shown in Figure 11b (and Table 1), the SR model results in larger retrieved ice particle effective diameters in comparison to the Smooth model. This trend of reduced COT and increased D_{eff} with the SR model appears consistent with previously observed effects of particle roughening on satellite retrievals [*Yang et al*., 2008; *Zhang et al*., 2009; *Baum et al*., 2011; *van Diedenhoven et al*., 2012] and with the lower COT values recently observed when testing the SR ASC model in MODIS retrievals (S. Platnick and M. D. King, personal communication). Nevertheless, although the effects on satellite and Sun photometer retrievals are related, the effects of crystal roughening on the backscattered light used by satellite retrievals are primarily due to the reduction of the asymmetry parameter, whereas our current retrieval scheme is directly affected by the first 2° forward scattered angles of the phase function.

[40] Comparison of the two LUTs in Figure 6 further delineates this result in using our retrieval method. As seen, the Smooth model results in larger COT values for the same data instance relative to the SR model. Also, since the Smooth model LUT is "shifted" to the higher transmittances domain for the VIS wavelengths, it allows only the relatively smaller COT retrievals to be valid. Since smaller COT values also tend to have D_{eff} values of ~80 μm, the overall median value for the Smooth model is smaller than the values obtained for the SR model.

[41] Ratios smaller than 1 are obtained for the two-component model (i.e., cirrus and smoke) as a result of incorporating aerosols in the calculation. The two-component model primarily impacts the retrieved D_{eff} values, in contrast to the COT retrievals. This has implications for the importance of retrievals under mixed scene conditions, and the need for a good representation of the mixed scene in terms of the aerosol characteristics. Nevertheless, as was demonstrated here, use of the clear sky measurements made by the Sun photometer itself can help to choose an appropriate aerosol model for the retrieval. This ability makes this platform attractive for cirrus COT and D_{eff} retrievals.

[42] A comparison of the retrievals using the three separate wavelength sets (Table 1) indicates that COT values and the number of valid retrievals do not differ much and that D_{eff} median value is slightly smaller for the two-wavelength retrieval scheme. When plotting the wavelength-dependent model based on two wavelengths for a specific data point (Figure 13a), the model spectral shape does not fit as well as the model chosen by nine-wavelength or six-wavelength models. It seems that by using a two-wavelength scheme, the retrieval is less constrained. The difference between the model fits for the six-wavelength or nine-wavelength cases is smaller and might suggest the former is a better candidate, since it reduces the uncertainty in matching bands that are heavily affected by gas absorption. Use of a chi-squared parameter as a quality measure of the fit when comparing the retrievals between the three wavelength sets is probably insufficient to determine which wavelength set is the most appropriate. Further comparison with other instruments or in situ measurements should shed more light on this decision.

[43] Although we observe that the retrieved ice cloud effective diameters have higher relative uncertainties than the retrieved COT, it is encouraging to see that the suggested approach has some sensitivity to this parameter. In a recent paper, *DeVore et al*. [2012] showed the ability of an imaging Sun photometer (SAM) to retrieve cirrus optical thickness and effective diameter (incorporating Baum-Yang 2005 smooth-faceted model [*Baum et al*., 2005b]) using solar disk radiance and aureole profiles together with forward RT calculations. However, in their comparison with MODIS cirrus products for four cases, SAM-retrieved cloud effective diameters of 180 μm were necessary to match with their model, where the MODIS derived values were in the range of 40–60 μm for all four cases.

[44] Unfortunately, for the 9 July case, there was no collocated MODIS overpass corresponding to the time of the measured cirrus clouds. However, a MODIS-Aqua overpass at 19:45 UT (with corresponding cloud-flagged AATS measurements at 17:00 UT and beyond 20:00 UT) is used (MODIS L2 MYD06 product was downloaded from http://mirador.gsfc.nasa.gov/) to compare with our retrieved range of D_{eff}. Figure 12a shows the same results as in Figure 11a, but as a function of latitude. The MODIS cirrus COT values for that specific granule were selected only for cirrus optical depth values below 4 (to represent the thin cirrus cases). In this case, all MODIS-retrieved COT values exceeded 1. Figure 12b presents the retrieved MODIS effective diameters for the corresponding COT cases shown in Figure 12a. MODIS-retrieved values are averaged over 0.2° latitude bins for clarity. In general, the retrieved D_{eff} values for this granule span the range of 10–100 μm (including retrieval uncertainty), although the majority of results is concentrated around 40–60 μm. We can see that both Smooth and SR models result in higher D_{eff} values, as was observed by *DeVore et al*. [2012] in their comparison with MODIS. The use of mainly smooth ice crystals of the *Baum et al*. [2005a, 2005b] model in the MODIS retrievals might lead to an overestimation of optical thickness and an underestimation of the effective diameter, if indeed rough ice crystals are assumed to be more realistic [*Yang et al*., 2008; *Zhang et al*., 2009; *Baum et al*., 2011; *van Diedenhoven et al*., 2012]. However, these biases were estimated to be substantially smaller than the observed differences between MODIS and our results.

[45] Nevertheless, it is interesting that a large cluster of retrieved values using the two-component model (i.e., cirrus and smoke) fall within the range of the MODIS retrieved values. This is also true for some of the retrieved points using the SR model. For valid retrievals that give D_{eff} values of 120 μm, there is a good spectral agreement between the measurements and the SR model (Figure 13b). Figures 13c and 13d demonstrate the chi-squared filtering method, where the former shows invalid retrievals for both models (chi-square above threshold of 0.001), and the latter shows how use of a two-component model yields a better fit (chi-square below threshold) to the measurements than does the use of the pure SR model (chi square above threshold). The addition of an aerosol model to the cirrus model increases the spectral slope beyond 600 nm and decreases transmittance in the VIS. Figure 13e shows an instance where both the SR and SR + smoke models are accepted as valid retrievals. In this case, the retrieved COT difference is 12% and the D_{eff}

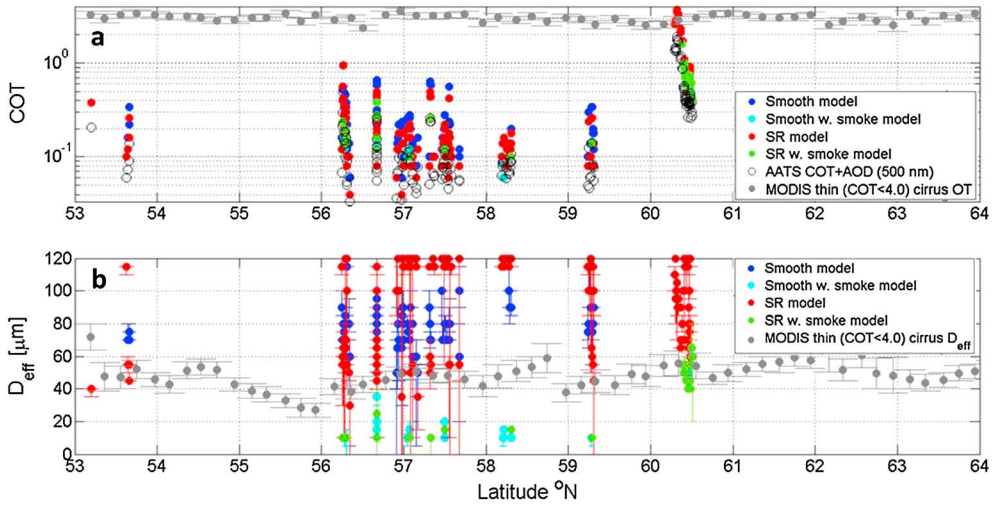

Figure 12. For 9 July 2008 ARCTAS case, valid retrieval values of (a) cirrus optical depth (COT) and (b) ice particle effective diameter similar to those shown in Figure 11, but as a function of latitude to allow comparison with MODIS-retrieved properties. Solid grey circles represent Aqua-MODIS (9 July, 19:45 UT granule) retrieved values (COT and ice particle effective diameter for thin cirrus cases with COT 4.0) averaged over 0.2° bins. MODIS overpass was not collocated with AATS flight path. MODIS retrieval algorithm uses *Baum et al.* [2005b] cirrus optical properties model of smooth-faceted ice particles.

difference is 33%. Our results indicate that in some instances, especially for low cirrus optical thicknesses (<1), the aerosol layer between the instrument and the cloud plays an important role. This conclusion might explain the discrepancy observed in some of the cloud effective diameter values retrieved by the SAM instrument and MODIS in *DeVore et al*. [2012]. Since their measurements were located at NASA GSFC, Maryland, which often has relatively large AOD [e.g., *Dubovik et al*., 2002], neglect of an appropriate amount of aerosol in their calculations may have resulted in an overestimation of the retrieved effective diameter. Another explanation for the discrepancy between the MODIS retrieved properties and the SAM instrument is that the measurement was obtained only for one visible wavelength, whereas the MODIS algorithm uses two wavelengths (one in the visible and one in the SWIR spectral region).

[46] Table 1 shows retrieval statistics for the different ice habit models (i.e., GHM as SR or Smooth, and MLT and ASC as severely roughened). Overall, there is no large difference between the models, both in retrieved COT and D_{eff} (range and median values) and the number of valid retrievals. However, when comparing corresponding data points, there is some difference in the D_{eff} values between the models, with the sign and magnitude of the difference showing no clear trends for the three models. Concurrent Sun photometer and in situ measurements are needed to examine which model would be more appropriate for such retrievals.

3.3. Mauna Loa Observatory (MLO)—29 September 2011—Ground-Based Case

[47] As shown for the 9 July 2008 ARCTAS case for very low COT values, the aerosol layer between the instrument and the cloud may play an important role in quantifying cloud properties, especially for absorbing aerosols. This implies that retrievals of cirrus properties from ground-based stations might be problematic unless the aerosol layer can be characterized somehow. This can be achieved by concurrent Sun photometer measurements of clear-sky AOD at the same location, assuming the values are relatively stable. Under very clean conditions that prevail at high altitude remote locations (e.g., MLO), where the aerosol layer can be well characterized and is usually stable and has absolute small AOD values, retrievals of cirrus properties might be more constrained when using ground-based Sun photometers. Potentially, this could increase the global coverage capability of cirrus measurements. In this section, we present results from the application of our methodology to measurements obtained at MLO, during one of our routine instrument calibration campaigns to demonstrate the feasibility of this approach for ground-based stations. Since the AOD values at MLO are very small (~0.02–0.05), the standard deviation filter and the a_1 method that is used for the ARCTAS data set do not result in a satisfactory separation of clouds from clear sky data. The use of the a_1 parameter suffers when the wavelength-dependent AOD spectra are difficult to represent with a quadratic fit due to the low AOD + COT values. Hence, we adopt the following screening method instead: data points for analysis are chosen based on the cases where the AOD values at 2138 nm were higher than the values at the 675 nm band, in addition to operator notes of visual cirrus occurrences. We find that data points chosen for our retrieval fall inside the LUT dual-wavelength transmittance domain as demonstrated in Figure 10 for the ARCTAS case. A deviation of data points is observed here as well in the LUT domain for COT < 0.3. To test the effect of an aerosol layer on the MLO retrievals, we use a two-component model of Smooth/SR cirrus models [*Baum et al*., 2011] with an aerosol model of tropical marine type (0% RH and a constant AOD contribution of 0.01 from OPAC). In Figure 14 we show the retrieved cirrus parameters, using the Smooth and SR ice models, and the corresponding two-component (cloud + aerosol) models. Table 2 summarizes the results for the MLO case. In general, COT values at MLO are less than those observed on 9 July during ARCTAS and

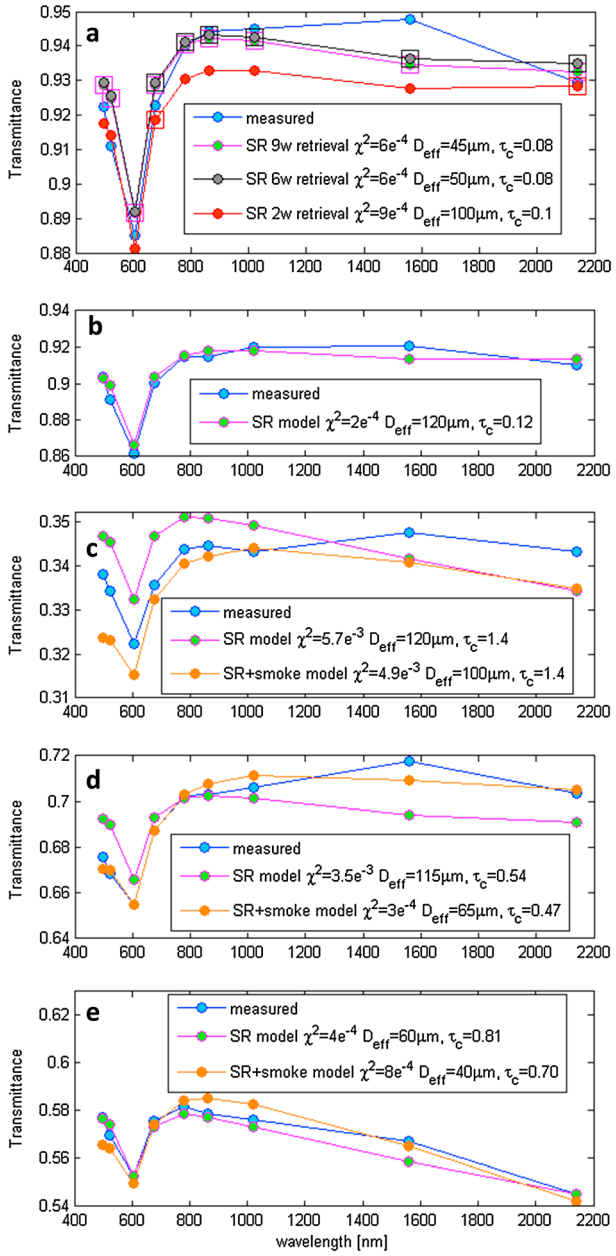

Figure 13. Sample spectra of measured and modeled non-Rayleigh transmittance values of (a) wavelength-dependent retrieval results comparing measured spectrum (light blue circles) with retrieved spectra resulting from nine-wavelength retrieval (solid green circles with magenta rectangles showing wavelengths used in retrieval), six-wavelength retrieval (solid grey circles with black rectangles showing wavelengths used in retrieval), and two-wavelength retrieval (solid red circles with red rectangles showing wavelengths used in the retrieval); and (b) valid retrieval case of D_{eff} = 120 μm with 2011 SR model as best fit, (c) invalid retrieval case of D_{eff} = 120 μm (both SR and SR + smoke models), (d) valid retrieval case of two-component model (SR + smoke), and (e) valid retrieval case of 2011 SR and SR + smoke models.

the highest values are around 1. The retrieved COT values for the Smooth model are slightly larger than the corresponding COT values for the SR model (according to median values), similar to our observations in the ARCTAS case (Figure 11a). The total COT + AOD values obtained by the non-corrected AATS retrieval algorithm are smaller than the corrected retrieved values, as expected. The ratio between the retrieved COT and the AATS values is somewhat similar to the values observed for the ARCTAS case, which is encouraging for the use of the Smooth and SR models for Sun photometer cirrus retrievals. The retrieved D_{eff} median values for both Smooth and SR models are smaller in general than the values obtained for the ARCTAS case. However, since the analyzed data set is relatively small, no conclusions can be drawn in terms of cirrus property comparisons between the two regions. A comparison of the two-component model with the pure cirrus model shows small differences in both COT and D_{eff} results (see Table 2), in contrast to the results obtained for the ARCTAS case (Table 1). The same is true with regard to the number of valid retrievals. This supports the hypothesis that in clean regions, cirrus retrievals might be more straightforward using ground-based Sun photometers.

[48] The fact that the number of valid retrievals for the MLO case is almost the same for both Smooth and SR models, in contrast to the ARCTAS case, makes it difficult to decide on the most appropriate model for cirrus retrievals by Sun photometers. However, the current analysis suggests that the Smooth model is better suited for COT smaller than 1, and the SR model is more appropriate for higher COT cases.

4. Summary and Conclusions

[49] Sun photometers are used globally to accurately measure aerosol optical depth when clouds do not obstruct the Sun's direct beam. When such obstruction occurs, however, the measured transmittance signal contains not only the direct transmitted term, but also the forward scattered contribution from the ice (or water) particles, which interferes with the proper derivation of total (cloud plus aerosol) optical depth via the simple Beer-Lambert relation. Earlier studies have suggested a solution to derivation of COT or AOD in the form of correction factors.

[50] In the present work, we propose a different approach that uses the additional information content that lies within the total measured irradiance below cirrus clouds to infer cirrus optical properties using Sun photometry. When cirrus is present, the measured irradiance includes not only the direct transmitted term but also a forward scattered component. This additional information, analyzed over a broad wavelength range (visible to SWIR spectral region), permits the derivation of spectral relationships that enhance the ability to retrieve COT and effective diameters for a specific set of cirrus optical properties.

[51] The suggested approach is tested on two cases: an airborne case that uses the AATS-14 airborne data on 1 day during the ARCTAS summer 2008 mission that involved cirrus over smoke, and a much less aerosol-laden case that uses AATS-14 ground-based data taken at Mauna Loa Observatory in Hawaii. Both cases show relatively small uncertainties in the retrieved COT but larger relative uncertainties with regard to the retrieved effective diameter values when using the various models and retrieval assumptions (i.e., a two-component model or various wavelengths sets).

[52] In comparing results assuming either Smooth or Severely Roughened (SR) cirrus optical models, we found

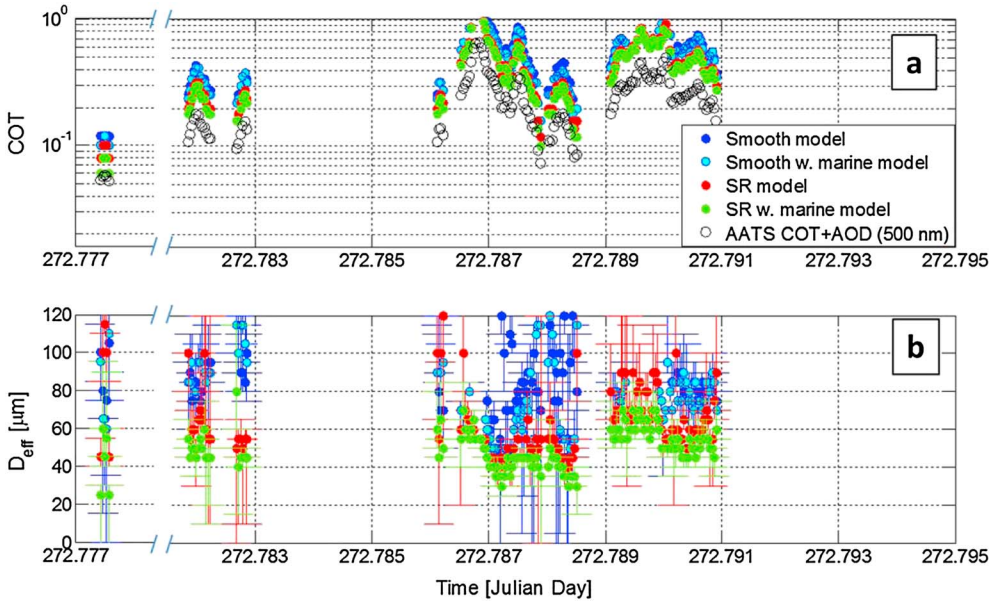

Figure 14. For 29 September 2011 MLO case, retrieved values of (a) cirrus optical depth for the *Baum et al.* [2011] Smooth model data set (solid blue circles), *Baum et al.* [2011] SR model data set (solid red circles), a two-component model including the Smooth model and a tropical marine aerosol model with constant AOD value of 0.01 (solid cyan circles), a two-component model including SR model and a tropical marine aerosol model with constant AOD value of 0.01 (solid green circles), and AATS total optical depth (which includes both COT and AOD at $\lambda = 500$ nm) for the corresponding cloud-flagged cases (open black circles); and (b) corresponding ice particle effective diameter values for the models shown in Figure 14a. Values are shown as a function of time (Julian day) for the MLO altitude of 3.4 km ASL.

that the latter produces a larger number of valid retrievals for a larger COT range. The SR model seemed to reflect better the differences among the different cases studied, with lower ice particle effective diameter retrieved for the smaller COT and vice versa for the higher COT. Nevertheless, for COT values below 1, both models produced almost the same results both in COT and ice particle effective diameter values. This is the first time where such a comparison was made with regard to the forward scattered part of these phase functions. Former investigations were concentrated on the response of remote sensing sensors to the backscattered values of these phase functions [e.g., [*Pierce et al.*, 2010; *Baum et al.*, 2011].

[53] Application of the retrieval scheme using different sets of wavelengths resulted in almost similar results for the retrieved COT values and the number of valid retrievals. When using only a two-wavelength scheme (VIS and SWIR channels), as is the standard for many cloud retrieval schemes to date, we observed slightly smaller D_{eff} values in comparison to retrievals that include more wavelengths (i.e., six-wavelength and nine-wavelength sets). It seems that since the fit is based only on two wavelengths, it is less constrained and can result in spectral mismatches when examined over the whole measurement spectral range. This observation is in accordance with a recently published water cloud retrieval scheme by *McBride et al.* [2011] who showed improved retrieval performance and stability when incorporating a spectral slope (using many wavelengths) in their water cloud retrieval algorithm.

[54] In comparing the LUTs of the various optical property cirrus models, we find that there is less variation among the mixed habit models (GHM, MLT, and TDC) than between the mixed habits and a model based on the use of a single habit: the severely roughened aggregate of solid columns (ASC). The ASC model was tested in our analysis since it may be adopted for use by the MODIS team in their new cloud retrieval collection 6 cloud products. Nevertheless, it was not confirmed to be the most probable particle type globally. Retrieval results using GHM, MLT, and the ASC models did not yield large differences in retrieved COT values, but showed differences in retrieved ice particle effective diameter values, without a clear trend. From the

Table 2. Summary Statistics for the MLO Case Retrievals Using the Smooth and SR 2011 Models

Model Used in Retrieval	Valid Retrievals (#)	COT[a]	D_{eff} [μm][b]	Retrieved COT/ AATS(COT + AOD)
Smooth	141	0.02–0.98 (0.36)	35–120 (80)	1.01–2.68
Smooth w. marine	150	0.02–1.20 (0.38)	40–120 (80)	0.79–2.54
SR (9w)	173	0.02–1.10 (0.34)	35–120 (60)	1.01–1.89
SR w. marine (9w)	165	0.02–1.20 (0.34)	10–100 (50)	0.65–1.85

[a]COT-retrieved values are given as range (min-max). Values in parenthesis are the median values.
[b]Ice particle effective diameter retrieved values are given as range (min-max). Values in parenthesis are the median values.

analysis made so far the choice of the appropriate model for Sun photometers is inconclusive. Further research will explore this issue more fully.

[55] We also conclude that the effect of an aerosol layer between the instrument and the cloud layer is important for yielding a more accurate retrieval, especially for optically thin cirrus layers ($\tau_c < 1.0$). For this, we show that the clear sky data measured by the Sun photometer can be used for the selection of the appropriate aerosol layer model. In our demonstration a constant AOD value is used in a two-component (cirrus and aerosol) LUT derivation. We also show that the simple total optical depth (cloud plus aerosol) retrieval algorithm used by AATS-14 for the cirrus-contaminated cases tends to underestimate the total optical depth (COT + AOD) values, in comparison to the current retrieval method. The ratio of the values between our retrieval method values and those from the AATS is not constant and excludes the option of a simple correction to the Sun photometer measurements to infer cirrus optical thickness values.

[56] In summary, the present approach can be used to increase the traceability and quantification of cirrus properties, which are important for many research fields in atmospheric science (e.g., radiation budgets, atmospheric chemistry, etc.). The ease and the relatively widespread use of Sun photometers globally, both as airborne and ground-based instruments, can contribute to increased capability of quantifying some of the most important cirrus properties such as cloud optical thickness and ice crystal effective diameter. To better understand the uncertainty in effective diameter retrieved values, there is still a need to conduct concurrent measurements with in situ cirrus particle samplers and imagers to test the retrieval sensitivity to the specific isolated particle habits and to extend the analysis data set to obtain more conclusive evidence over different geographical regions.

[57] **Acknowledgments.** Michal Segal-Rosenheimer would like to thank the ORAU (Oak-Ridge Associated Universities) NPP (NASA Post-doctoral Program) and the Weizmann Institute through the Women in Science program for the financial support for her Post-doctoral fellowship at the NASA Ames Research Center. S Ramachandran would also like to thank ORAU-NPP for his support. The ARCTAS measurements were supported by the NASA Radiation and Science Program. We appreciate the comments of the three anonymous reviewers, which helped us to improve the manuscript.

References

Baum, B. A., P. Yang, A. J. Heymsfield, and S. T. Bedka (2005a), Bulk scattering properties for the remote sensing of ice clouds. Part I: Microphysical data and models, *J. Appl. Meteorol.*, *44*(12), 1885–1895.

Baum, B. A., P. Yang, A. J. Heymsfield, S. Platnick, M. D. King, Y.-X. Hu, and S. T. Bedka (2005b), Bulk scattering properties for the remote sensing of ice clouds. Part II: Narrowband models, *J. Appl. Meteorol.*, *44* (12), 1896–1911.

Baum B. A., P. Yang, A. J. Heymsfield, C. G. Schmitt, Y. Xie, A. Bansemer, Y. X. Hu, and Z. Zhang (2011), Improvements in shortwave bulk scattering and absorption models for the remote sensing of ice clouds, *J. Appl. Meteorol. Clim.*, *50*, 1037–1056, doi:10.1175/2010JAMC2608.1.

Chiu, J. C., C.-H. Huang, A. Marshak, I. Slutsker, D. M. Giles, B. N. Holben, Y. Knyazikhin, and W. J. Wiscombe (2010), Cloud optical depth retrievals from the Aerosol Robotic Network (AERONET) cloud mode observations, *J. Geophys. Res.*, *115*, D14202, doi:10.1029/2009JD013121.

Cole, B., P. Yang, B. A. Baum, J. Riedi, L. Labonnote, F. Thieuleux, and S. Platnick (2013), Comparison of PARASOL observations with polarized reflectances simulated using different ice habit mixtures, *J. Appl. Meteor. Clim.*, *52*, 186–196, doi:http://dx.doi.org/10.1175/JAMC-D-12-097.1

Comstock J. M., et al. (2007), An intercomparison of microphysical retrieval algorithms for upper tropospheric ice clouds, *Am. Meteorol. Soc.*, *191–204*, doi:10.1175/BAMS-88-2-191.

DeMott P. J., A. J. Prenni, X. Liu, S. M. Kreidenweis, M. D. Pettersa, C. H. Twohy, M. S. Richardsona, T. Eidhammer, and D. C. Rogers (2010), Predicting global atmospheric ice nuclei distributions and their impacts on climate, *PNAS*, *107*(25), 11217–11222, doi:10.1073/pnas.0910818107.

DeVore, J. G., A. T. Stair Jr., A. J. LePage, and D. Villanucci (2012), Using scattering calculations to compare MODIS retrievals of thin cirrus optical properties with SAM solar disk and aureole radiance measurements, *J. Geophys. Res.*, *117*, D01204, doi:10.1029/2011JD015858.

Dubovik, O., B. N. Holben, T. F. Eck, A. Smirnov, Y. J. Kaufman, M. D. King, D. Tanré, and I. Slutsker (2002), Variability of absorption and optical properties of key aerosol types observed in worldwide locations, *J. Atmos. Sci.*, *59*, 590–608

Dunagan, S., R. Johnson, J. Zavaleta, R. Walker, C. Chang, P. Russell, B. Schmid, C. Flynn, and J. Redemann (2011), 4STAR Spectrometer for Sky-Scanning Sun-Tracking Atmospheric Research: Instrument technology development, Preprint, 34th International Symposium on Remote Sensing of Environment, Sydney, Australia

Gao B. C., K. Meyer, and P. Yang (2004), A new concept on remote sensing of cirrus optical depth and effective ice particle size using strong water vapor absorption channels near 1.38 and 1.88 μm, *IEEE Trans. Geosci. Remote Sens.*, *42*(9), doi:10.1109/TGRS.2004.833778.

Garnier, A., J. Pelon, P. Dubuisson, M. Faivre, O. Chomette, N. Pascal, and D. Kratz (2012), Retrieval of cloud properties using CALIPSO imaging infrared radiometer, Part I: Effective emissivity and optical depth, doi:10.1175/JAMC-D-11-0220.1.

Hair, J. W., C. A. Hostetler, A. L. Cook, D. B. Harper, R. A. Ferrare, T. L. Mack, W. Welch, L. R. Izquierdo, and F. E. Hovis (2008), Airborne high spectral resolution lidar for profiling aerosol optical properties, *Appl. Opt.*, *47*, 6734–6752, doi:10.1364/AO.47.006734, 2008

Hess M., P. Koepke, and I. Schult (1998), Optical properties of aerosols and clouds: The software package OPAC, *Bull. Am. Meteorol. Soc.*, *79*(5), 831–844.

Holben, B. N., et al. (2001), An emerging ground-based aerosol climatology: Aerosol optical depth from AERONET, *J. Geophys. Res.*, *106*, 12067–12097.

Jacob D. J., et al. (2010), The Arctic Research of the Composition of the Troposphere from Aircraft and Satellites (ARCTAS) mission: Design, execution, and first results, *Atmos. Chem. Phys.*, *10*, 5191–5212, doi:10.5194/acp-10-5191-2010.

Kinne S., T. P. Akerman, M. Shiobara, A. Uchiyama, A. J. Heymsfield, L. Miloshevich, J. Wendell, E. W. Eloranta, C. Purgold, and R. W. Bergstrom (1997), Cirrus cloud radiative and microphysical properties from ground observations and in situ measurements during FIRE 1991 and their application to exhibit problems in cirrus solar radiative transfer modeling, *J. Atmos. Sci.*, *54*, 2320–2341.

Liou, K. N. (1986), Influence of cirrus clouds on weather and climate processes—A global perspective, *Mon. Wea. Rev.*, *114*, 1167–1199.

McBride P. J., K. S. Schmidt, P. Pilewskie, A. S. Kittelman, and D. E. Wolfe (2011), A spectral method for retrieving cloud optical thickness and effective radius from surface-based transmittance measurements, *Atmos. Chem. Phys.*, *11*, 7235–7252, doi:10.5194/acp-11-7235-2011.

Nakajima, T., and M. D. King (1990), Determination of the optical thickness and effective particle radius of clouds from reflected solar radiation measurements. Part I: Theory, *J. Atmos. Sci.*, *47*, 1878–1893.

Nazaryan H., M. P. McCormick, and W. P. Menzel (2008), Global characterization of cirrus clouds using CALIPSO data, *J. Geophys. Res.*, *113*, D16211, doi:10.1029/2007JD009481.

O'Neill, N. T., T. F. Eck, A. Smirnov, B. N. Holben, and S. Thulasiraman (2003), Spectral discrimination of coarse and fine mode optical depth, *J. Geophys. Res.*, *108*, D17, 4559, doi:10.1029/2002JD002975.

Pierce J. R., R. A. Kahn, M. R. Davis, and J. M. Comstock (2010), Detecting thin cirrus in multiangle imaging spectroradiometer aerosol retrievals, *J. Geophys. Res.*, *115*, D08201, doi:10.1029/2009JD013019.

Platnick, S., M. D. King, S. A. Ackerman, W. Paul Menzel, B. A. Baum, and R. A. Frey (2003), The MODIS cloud products: Algorithms and examples from Terra, *IEEE Trans. Geosci. Remote Sens.*, *41*, 459–473, doi:10.1109/TGRS.2002.808301.

Russell P. B., et al. (1993), Pinatubo and pre-Pinatubo optical-depth spectra: Mauna Loa measurements, comparisons, inferred particle size distributions, radiative effects, and relationship to lidar data, *J. Geophys. Res.*, *98*(D12), 22,969–22,985.

Russell P. B., J. M. Livingston, O. Dubovik, S. A. Ramirez, J. Wang, J. Redemann, B. Schmid, M. Box, and B. N. Holben (2004), Sunlight transmission through desert dust and marine aerosols: Diffuse light corrections to Sun photometry and pyrheliometry, *J. Geophys. Res.*, *109*, D08207, doi:10.1029/2003JD004292.

Russell, P. B., et al. (2005), Aerosol optical depth measurements by airborne Sun photometer in SOLVE II: Comparisons to SAGE III, POAM

III and airborne spectrometer measurements, *Atmos. Chem. Phys.*, *5*, 1311–1339, SRef-ID:1680-7324/acp/2005-5-1311

Schmid, B., et al. (2011), 4STAR Spectrometer for Sky-Scanning Sun-Tracking Atmospheric Research: Results from test-flight Series, Paper A14E-05, American Geophysical Union Fall Meeting, San Francisco.

Seifert, P., et al. (2011), Ice formation in ash-influenced clouds after the eruption of the Eyjafjallajökull volcano in April 2010, *J. Geophys. Res.*, *116*, D00U04, doi:10.1029/2011JD015702.

Shinozuka, Y., et al. (2011), Airborne observation of aerosol optical depth during ARCTAS: Vertical profiles, intercomparison and fine-mode fraction, *Atmos. Chem. Phys.*, *11*, 3673–3688, doi:10.5194/acp-11-3673-2011

Shinozuka, Y., and J. Redemann (2011), Horizontal variability of aerosol optical depth observed during the ARCTAS airborne experiment, *Atmos. Chem. Phys.*, *11*, 8489–8495, 2011, www.atmos-chem-phys.net/11/8489/2011/, doi:10.5194/acp-11-8489.

Shiobara M., and S. Asano (1994), Estimation of cirrus optical thickness from Sun-photometer measurements, *J. Appl. Meteorol.*, *33*, 672–681.

Takano, Y., and K. N. Liou (1989), Solar radiative transfer in cirrus clouds. Part I: Single-scattering and optical properties of hexagonal ice crystals, *J. Atmos. Sci.*, *46*, 3–19.

van Diedenhoven, B., A. M. Fridlind, A. S. Ackerman, and B. Cairns (2012), Evaluation of hydrometeor phase and ice properties in cloud-resolving model simulations of tropical deep convection using radiance and polarization measurements, *J. Atmos. Sci.*, *69*, 3290–3314, doi: http://dx.doi.org/10.1175/JAS-D-11-0314.1

Wylie, D. P., and W. P. Menzel (1999), Eight years of high cloud statistics using HIRS, *J. Climate*, *12*, 170–184.

Yang P., G. Hong, G. W. Kattawar, P. Minnis, and Y. Hu (2008), Uncertainties associated with the surface texture of ice particles in satellite-based retrieval of cirrus clouds: Part II—Effect of particle surface roughness on retrieved cloud optical thickness and effective particle size, *IEEE Trans. Geo. Remote Sens.*, *46*(7), 1948–1957, doi:10.1109/TGRS.2008.916472.

Zhang Z., P. Yang, G. Kattawar, J. Riedi, L. C. Labonnote, B. A. Baum, S. Platnick, and H.-L. Huang (2009), Influence of ice particle model on satellite ice cloud retrieval: Lessons learned from MODIS and POLDER cloud product comparison, *Atmos. Chem. Phys.*, *9*, 7115–7129, www.atmos-chem-phys.net/9/7115/2009/